applied sciences

MDPI

Article

Path Asymmetry in Soil Water Retention: The State Resilience Index (SRI) as a Transferable Hysteresis Descriptor

Pellegrino Conte

Department of Agricultural, Food and Forest Sciences, University of Palermo, v.le delle Scienze Building 4, 90128 Palermo, Italy; pellegrino.conte@unipa.it

Featured Application

The State Resilience Index (SRI) can be applied as a rapid, model-free diagnostic tool for the pedological characterization and environmental monitoring of soil structural state. Derived directly from hysteresis data embedded in soil water retention curves or water vapor sorption isotherms, SRI quantifies hydraulic path asymmetry as a single dimensionless descriptor, without requiring curve fitting or model assumptions. Its responsiveness to pedogenic differentiation across soil horizons, mineralogical composition, and progressive structural alteration under repeated hydraulic cycling positions SRI as a broadly transferable index for comparative soil assessments across contrasting pedoclimatic environments. Potential applications include the monitoring of soil structural degradation under land use change, the characterization of depth-dependent hydraulic complexity in soil profiles, and the integration of SRI into multi-indicator frameworks for soil quality and ecosystem function assessment.

Abstract

Soil hydraulic hysteresis—the divergence between drying and wetting trajectories of the water retention curve—encodes quantitative information on soil structural organization that traditional modelling approaches do not explicitly capture. This study introduces the State Resilience Index (SRI), a dimensionless descriptor defined as the normalized area enclosed between the drying and wetting branches of a hysteresis loop and evaluates its interpretive value across five contrasting datasets from the published literature. The datasets encompass compaction gradients, repeated wetting–drying cycles, depth-resolved soil profiles, and water vapor sorption isotherms from soils differing in clay content and mineralogy. SRI values ranged from 0.023 to 0.333, responding consistently to the dominant structural drivers of hysteresis in each system. High values were associated with heterogeneous, structurally complex pore networks characteristic of productive soils; declining values reflected progressive loss of structural memory under compaction, repeated cycling, or mineralogical rigidity. A provisional interpretive framework is proposed, linking SRI ranges to soil structural quality and agronomic potential. The index is dimensionless, model-free, and applicable across measurement domains and forcing regimes, positioning it as a broadly transferable tool for the comparative assessment of soil hydraulic path asymmetry.

Keywords: soil hydraulic hysteresis; water retention curve; soil structural quality; pore network heterogeneity; dimensionless index; vapor sorption isotherm; soil health monitoring

Check for updates

Received: 2 June 2026
Revised: 18 June 2026
Accepted: 22 June 2026
Published: 3 July 2026

1. Introduction

Water retention and release processes in soils are inherently path-dependent. The relationship between water content (θ) and matric potential (h) follows distinct trajectories during drying and wetting, resulting in the well-known phenomenon of hydraulic hysteresis. This behavior has been widely documented and attributed to multiple interacting mechanisms, including pore network geometry, ink-bottle effects, contact angle variability, entrapped air, and structural rearrangements occurring during wetting–drying cycles [1–3].

Despite decades of research, hysteresis is still primarily treated either as a modelling complication or as a phenomenological feature of soil hydraulic behavior, rather than as a source of quantitative information on soil state and structural organization. Traditional approaches typically focus on fitting primary or scanning curves, or on introducing empirical or semi-empirical corrections into constitutive models [3,4]. While these frameworks are effective for prediction, they do not directly provide a compact descriptor of the divergence between wetting and drying trajectories, nor do they explicitly quantify the degree to which a soil system departs from reversible behavior [5].

From a physical standpoint, hysteresis reflects the incomplete recovery of the system state along a given hydraulic path. In other words, the soil does not retrace the same configuration when subjected to inverse boundary conditions. This path dependence emerges from a combination of structural constraints and dynamic processes, including pore-scale connectivity, phase distribution, and local energy barriers controlling fluid redistribution [6,7]. As such, hysteresis can be interpreted not merely as a deviation between curves, but as an integrated signature of how the soil system evolves between states under changing hydraulic conditions [7,8].

Beyond its geometrical manifestation, hysteresis can be interpreted as the macroscopic expression of thermodynamic irreversibility. When a soil undergoes a wetting–drying cycle, the forward and backward trajectories generally traverse different metastable configurations and therefore do not retrace the same path. The resulting hysteresis loop is not merely a geometric divergence between curves, but the observable signature of energy dissipation and entropy production during the cycle. This perspective suggests that hysteresis may contain quantitative information on the persistence of soil state beyond that captured by conventional hydraulic descriptors.

In this context, there is a growing need for simple, transferable metrics capable of capturing the magnitude of path dependence in a way that is comparable across soils, experimental conditions, and scales. Existing descriptors—such as scanning loop ratios, reversal points, or curve-fitting residuals—are often dataset-specific and lack a clear normalization framework, limiting their use for cross-study comparisons [5,9].

The most directly related precedent is the hysteresis index proposed by Gebrenegus and Ghezzehei [5], which quantifies the degree of hysteresis as the ratio of the air-entry value on the wetting curve to that on the drying curve—a single-point, parameter-based metric derived from fitted van Genuchten curves. While this index provides a useful scalar summary of hysteresis at the characteristic inflection point, it carries three inherent limitations. First, it is anchored to a specific model parameterization, requiring prior fitting of the van Genuchten equation to both branches and therefore inheriting all associated assumptions and fitting uncertainties. Second, being defined at a single point of the retention curve (the air-entry pressure), it does not capture the integrated divergence between branches across the full hydraulic range. Third, and most importantly, its formulation is restricted to the matric potential domain of the soil water retention curve and cannot be extended to other forcing variables—such as relative humidity in vapor sorption isotherms—without loss of physical meaning. The State Resilience Index proposed here differs from this approach in three corresponding respects: it is entirely model-free, requiring no curve fitting;

it integrates the divergence between branches over their full common domain; and its normalization structure is indifferent to the nature of the forcing and observable variables, making it directly applicable across hydraulic regimes and measurement domains.

To address this gap, the State Resilience Index (SRI) is introduced here. This is a dimensionless descriptor derived from the normalized area enclosed between drying and wetting branches of the soil water retention curve. By construction, SRI quantifies the divergence between forward and backward hydraulic trajectories, providing a continuous measure of path dependence that ranges from nearly reversible behavior (values approaching zero) to strongly asymmetric responses (values approaching unity). Importantly, SRI does not aim to describe adsorption strength or water retention capacity per se, but rather the extent to which the system preserves the imprint of its hydraulic pathway.

The conceptual foundation of SRI lies in the interpretation of hysteresis as a manifestation of state persistence under external forcing. Within this framework, higher SRI values indicate a stronger divergence between trajectories, suggesting that the system retains a pronounced dependence on its prior configuration. Conversely, low SRI values are associated with more reversible responses, where wetting and drying paths converge and the system exhibits limited path asymmetry.

The objective of this study is to evaluate the interpretive and comparative value of SRI across a range of soil systems characterized by distinct pedo-physical drivers of hysteresis. Specifically, the index has been applied to previously published datasets encompassing (i) wetting–drying cycling effects, (ii) soil compaction and porosity alteration, (iii) mineralogical controls, and (iv) depth-dependent structural variations. By analyzing these contrasting scenarios within a unified framework, it will be assessed whether SRI can consistently capture meaningful differences in hydraulic behavior and provide insight into the underlying mechanisms governing path-dependent responses. The present study therefore aims to evaluate whether SRI can serve as a transferable descriptor of hydraulic path asymmetry, with potential applications in comparative soil physics, structural assessment, and the interpretation of dynamic soil–water interactions across heterogeneous systems.

2. Theoretical Background

2.1. The Thermodynamic State of Water and the Role of Water Activity

The thermodynamic state of water in any system—whether a soil pore network, a vapor sorption isotherm, or a colloidal suspension—is fully described by its chemical potential μ_w, which quantifies the free energy per mole of water at given temperature T and pressure P. For a system in contact with a vapour phase, μ_w is related to the dimensionless water activity a_w by:

$$\mu_w(T, P) = \mu_w(T) + RT \ln a_w \quad (1)$$

where $\mu_w(T)$ is the chemical potential of pure liquid water at temperature T and reference pressure (1 bar), and R is the universal gas constant. In soil physics and hydrology, the same thermodynamic information is conventionally expressed through the matric potential ψ (J kg^{-1}), defined as the work required to transfer a unit mass of water from the soil matrix to a reference state of pure free water. The two quantities are related by the linear transformation:

$$\psi = \left(\frac{RT}{M_w}\right) \ln a_w \quad (2)$$

where $M_w = 0.018015\ \mathrm{kg\ mol^{-1}}$ is the water molar mass. Equation (2) establishes that ψ and $\ln a_w$ are proportional at constant temperature: they carry identical physical information, differing only in units and historical conventions. This proportionality has a direct and non-trivial consequence for the SRI, which is discussed in Section 2.4.

In an ideal, reversible process at constant T and P, the Gibbs free energy G is minimized at equilibrium, and its cyclic integral vanishes:

$$\oint dG = 0 \quad (3)$$

Under this condition, forward and backward trajectories of the system in any response–forcing plane (Figure 1) coincide exactly, and no hysteresis is observed. Real porous systems deviate from this ideal because their free-energy landscape is not a single smooth valley but a rugged surface populated by multiple metastable local minima separated by energy barriers [10]. As the external forcing changes direction, the system traces different paths through this landscape, visiting different metastable configurations during wetting and drying. This directional asymmetry is the physical origin of hysteresis.

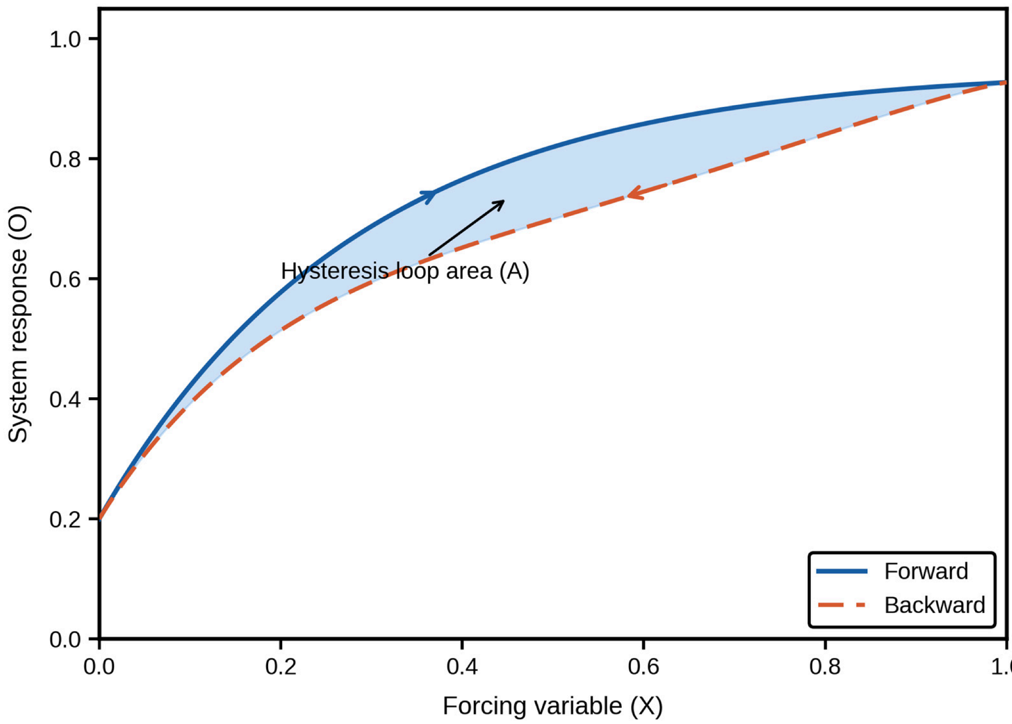

Figure 1. Example of a hysteresis loop. The area between the two branches measures the intensity of the dynamic hysteretic range; O, and X are the observable parameter and the forcing variable, respectively.

2.2. Irreversibility, Entropy Production, and the Dissipated Work

For a closed system subjected to a cyclic variation of water content θ and returning to the same macroscopic state at the end of each cycle, the cyclic integral of G vanishes because G is a state function (Equation (3)).

This is consistent with irreversibility. However, the second law of thermodynamics requires that entropy is produced internally (S_{int}) during any irreversible cycle [11]:

$$\Delta S_{irrev} = \oint dS_{int} > 0 \quad (4)$$

This internally produced entropy corresponds to energy irreversibly released as heat to the thermal reservoir. During the forward branch (wetting), the system absorbs work from the environment; during the backward branch (drying), it returns a smaller amount. The difference—equal to the area enclosed by the hysteresis loop (Figure 1)—constitutes the net energy dissipated per cycle.

For an isothermal process in which the conjugate variables are water content θ and $\ln a_w$, the net work exchanged over the cycle is:

$$W_{net} = \oint \mu_w d\theta \tag{5}$$

Substituting Equation (1) and noting that $\oint \mu_w d\theta = 0$ because θ returns to its initial value over the closed cycle:

$$E_{diss} = RT \oint \ln a_w d\theta \geq 0 \tag{6}$$

The quantity E_{diss} is the energy irreversibly dissipated per cycle per unit mass of dry solid (J kg^{-1}). It is strictly positive for any irreversible process and equals zero only for a perfectly reversible one. Geometrically, it corresponds to the oriented area of the hysteresis loop in the $(\theta, \ln a_w)$ plane.

2.3. Normalization and Definition of the State Resilience Index (SRI)

The dissipated energy E_{diss} given in Equation (6) depends on the specific experimental conditions: two systems with identical hysteretic tendency but operating over different ranges of θ and a_w will yield different absolute loop areas. To obtain a transferable, dimensionless descriptor, E_{diss} must be normalised by the maximum energy that could theoretically be dissipated under the same experimental conditions.

Define the dynamic ranges of the forcing and response variables over the common measurement domain:

$$\Delta\theta = \theta_{max} - \theta_{min} \tag{7}$$

$$\Delta(\ln a_w) = \ln a_{w,max} - \ln a_{w,min} \tag{8}$$

The maximum possible value of $\left|\oint \ln a_w d\theta\right|$ is attained when the forward branch lies entirely on one side of the rectangle $[\theta_{min}, \theta_{max}] \times [\ln a_{w,min}, \ln a_{w,max}]$ and the backward branch on the opposite side:

$$\left|\oint \ln a_w d\theta\right|_{max} = \Delta\theta \cdot \Delta(\ln a_w) \tag{9}$$

This is the area of the bounding rectangle. No hysteresis loop can exceed it, because neither θ nor $\ln a_w$ can exit their own experimental dynamic range. The bounding rectangle is therefore not an arbitrary geometric construct: it represents the maximum accessible phase space of the system under the given conditions, and its area is the maximum irreversible work that the system could dissipate per cycle.

The State Resilience Index is defined as the ratio of the actual dissipated energy to this maximum:

$$SRI = \frac{\left|\oint \ln a_w d\theta\right|}{\Delta\theta \cdot \Delta(\ln a_w)} \tag{10}$$

For systems in which the two branches intersect—generating lobes of opposite sign that would partially cancel in the oriented integral—the numerator is replaced by the absolute area:

$$A_n = \int_{\theta_{min}}^{\theta_{max}} \left|\ln a_{w,f(\theta)} - \ln a_{w,b(\theta)}\right| d\theta \tag{11}$$

Here, f and b stand for forward and backward, thereby referring to the two branches of the hysteretic cycle. Therefore, the general definition becomes:

$$SRI = \frac{A_n}{\Delta\theta \cdot \Delta(\ln a_w)} \tag{12}$$

https://doi.org/10.3390/app16136667

By construction, SRI ∈ [0, 1]: a value of zero corresponds to a perfectly reversible process, and a value approaching unity would indicate that the full accessible phase space is swept by path asymmetry. The computational implementation uses Equation (12), evaluated numerically via trapezoidal integration on a common resampled grid (Section 3). Finally, it must be noticed that the term "resilience" in the index name is used here in a strictly thermodynamic sense: it refers to the capacity of the system to preserve the imprint of its prior hydraulic state across a forcing cycle, as quantified by the fraction of irreversible work dissipated relative to the thermodynamic maximum. This usage carries no ecological or engineering connotation of recovery after disturbance.

2.4. Invariance of SRI Under the Transformation from Water Activity to Matric Potential

Soil water retention curves are measured and reported in terms of matric potential ψ rather than $\ln a_w$. The relationship between the two is the linear transformation given in Equation (2). Because this transformation is linear, the loop area in the (θ, ψ) plane is related to that in the $(\theta, \ln a_w)$ plane by a constant multiplicative factor:

$$\int \left|\psi_{f(\theta)} - \psi_{b(\theta)}\right| d\theta = \left(\frac{RT}{M_w}\right) \cdot A_n \tag{13}$$

Substituting into the definition of SRI and noting that $\Delta\psi = (RT/M_w) \cdot \Delta(\ln a_w)$, the constant RT/M_w cancels exactly in the ratio:

$$SRI = \frac{\left|\int \left|\psi_{f(\theta)} - \psi_{b(\theta)}\right| d\theta\right|}{\Delta\theta \cdot \Delta\psi} \tag{14}$$

This invariance is not a coincidence: it follows directly from the linearity of the transformation between the two thermodynamic potentials. SRI computed from a (θ, ψ) retention curve is numerically identical to SRI computed from the corresponding $(\theta, \ln a_w)$ sorption isotherm. The index is therefore not anchored to a particular choice of thermodynamic variable: it is a property of the hysteresis loop, expressible equivalently in any linearly related representation of the water potential.

This invariance also clarifies the physical meaning of the normalization by $\Delta\theta \cdot \Delta O$ (where O denotes the observable, whether ψ or $\ln a_w$): the denominator always represents the maximum accessible phase space of the system in the chosen representation, and the ratio always expresses the fraction of that space swept by path asymmetry. The bounding rectangle is not a geometric approximation of the true accessible state space; it is its exact definition under the given experimental conditions, and its area is the thermodynamic maximum of irreversible work per cycle.

3. Materials and Methods

3.1. Dataset Selection

The literature search was conducted using Web of Science and Scopus, with the following search strings: 'soil water retention hysteresis', 'soil hydraulic hysteresis', 'water vapour sorption hysteresis soil', and 'wetting drying cycles soil'. The search covered publications from 1970 to 2025. Additional references were identified through citation tracking of key papers retrieved in the primary search.

Published studies were selected based on their suitability for consistent reconstruction and comparison of hydraulic hysteresis. The aim of the selection was not to provide an exhaustive review of the literature on soil water retention hysteresis, but to identify datasets allowing a robust and reproducible calculation of the State Resilience Index (SRI) across contrasting pedo-physical conditions.

To be included, a study had to satisfy four conditions: (i) explicit reporting of both drying and wetting branches of the water retention relationship; (ii) sufficient graphical resolution to allow reliable extraction of the two trajectories; (iii) adequate overlap between branches over a common domain of the forcing variable; and (iv) clear experimental context enabling interpretation of the dominant driver of hysteresis. On this basis, the final set of datasets was chosen to represent distinct sources of hydraulic path asymmetry, including repeated drying–wetting cycling, compaction, mineralogical contrast, and depth-dependent structural variation.

Several additional studies were screened but not retained because they reported only fitted curves, incomplete hysteresis loops, insufficient graphical detail, or datasets whose structure did not permit meaningful cross-case comparison. The selected studies should therefore be regarded as a purpose-driven set of methodologically compatible cases, rather than as a statistically representative sample of the full literature. Table 1 reports the datasets used in the present paper, together with the SRI values and standard deviations (for the calculation procedure, the reader is addressed to the paragraph below).

Table 1. State Resilience Index (SRI) values and associated standard deviations obtained from digitized hysteresis datasets used in this study. Reported systems include bulk-density contrasts, depth-resolved soil profiles, repeated drying–wetting cycles, and water-vapour sorption isotherms from soils with contrasting clay contents and mineralogy. Values are means from Monte Carlo simulations (N = 1000); SD = standard deviation.

Reference Study	Source Figure in the Cited Study	System/Condition	SRI	SD
Rafraf et al. 2016 [12]	Figure 1a	ρ_d = 0.79 g cm^{-3} (slurry)	0.294	0.003
Rafraf et al. 2016 [12]	Figure 1b	ρ_d = 1.35 g cm^{-3} (compacted)	0.041	0.003
Rafraf et al. 2016 [12]	Figure 1c	ρ_d = 1.53 g cm^{-3} (compacted)	0.031	0.003
Shein & Mady 2018 [13]	Figure 1a	0–10 cm; ρ_d = 1.18 g cm^{-3}	0.093	0.005
Shein & Mady 2018 [13]	Figure 1b	10–20 cm; ρ_d = 1.25 g cm^{-3}	0.112	0.006
Shein & Mady 2018 [13]	Figure 1c	30–40 cm; ρ_d = 1.40 g cm^{-3}	0.116	0.005
Shein & Mady 2018 [13]	Figure 1d	40–50 cm; ρ_d = 1.49 g cm^{-3}	0.055	0.005
Wen et al. 2020 [14]	Figure 3b	1st drying–wetting cycle	0.333	0.005
Wen et al. 2020 [14]	Figure 3b	2nd drying–wetting cycle	0.230	0.005
Wen et al. 2020 [14]	Figure 3b	3rd drying–wetting cycle	0.130	0.007
Wen et al. 2020 [14]	Figure 3b	4th drying–wetting cycle	0.054	0.006
Wen et al. 2020 [14]	Figure 3b	5th drying–wetting cycle	0.023	0.005
Arthur et al. 2015 [15]	Figure 2	46% clay	0.098	0.002
Arthur et al. 2015 [15]	Figure 2	19% clay	0.128	0.004
Arthur et al. 2019 [16]	Figure 1	Smectite-rich sample	0.082	0.001
Arthur et al. 2019 [16]	Figure 1	Illite-rich sample	0.080	0.002
Arthur et al. 2019 [16]	Figure 1	Kaolinite-rich sample	0.049	0.002

3.2. Data Digitization

The drying and wetting branches of each selected curve were extracted from the original published figures using WebPlotDigitizer (https://automeris.io/wpd/ (accessed on 1 June 2026)). For each dataset, the axes were calibrated directly on the source figure, and the two branches were digitized separately. Care was taken to preserve the original scale of the forcing variable, which was treated as linear or logarithmic depending on the representation adopted in the source study. This distinction was retained throughout the subsequent numerical treatment. In the R workflow (v4.5.1), log-scaled datasets were transformed into log10(x) before interpolation and integration, whereas linearly reported datasets were analyzed in their original scale.

The digitized values were then organized into spreadsheets and processed in R. In the case of water vapor sorption datasets, the adsorption branch was operationally treated as the wetting path and the desorption branch as the drying path, in order to preserve a common hysteretic interpretation across all systems. This correspondence is explicitly encoded in the analysis scripts for the Arthur et al. [15,16] datasets.

3.3. Numerical Reconstruction of Hysteresis Loops

For each dataset, the digitized wetting and drying branches were interpolated onto a common support using piecewise linear interpolation. The integration domain was restricted to the interval over which both branches overlapped in order to avoid artificial closure of the cycle outside the experimentally documented range.

More specifically, if x_{wet} and x_{dry} denote the forcing coordinates of the two branches, the common interval was defined by the largest lower bound and the smallest upper bound of the two domains. Within this interval, both branches were resampled over a regular grid of 500 points, a resolution used consistently across all R scripts.

Hysteresis area A was computed numerically as the integral of the absolute difference between the interpolated drying and wetting branches over the common grid, using the trapezoidal rule. This procedure yields a direct numerical estimate of the loop area while remaining independent of any parametric curve fitting. Moreover, this approach implicitly accommodates the common experimental situation in which the drying and wetting branches do not close at the wet end due to entrapped air or incomplete saturation: since integration is restricted to the experimentally documented overlap interval, no artificial closure is imposed and the loop area reflects only the path asymmetry actually observed within the measured range.

3.4. Definition and Normalization of the State Resilience Index

In the computational workflow, SRI was evaluated using Equation (12) of the Theoretical Background (Section 2), with the hysteresis area A_n computed via trapezoidal integration over the common resampled grid described in Section 3.3. The dynamic range ΔO was computed as the difference between the maximum and minimum values of the two interpolated branches taken together over the common interval, and ΔX as the width of that interval. This normalization expresses hysteresis as the fraction of the accessible phase space swept by path asymmetry, allowing direct comparison across datasets obtained with different variables, scales, and forcing ranges. For datasets reported on a logarithmic forcing axis, ΔX was computed in log10 units consistently with the transformation applied prior to interpolation.

3.5. Monte Carlo Estimation of Uncertainty

To evaluate the numerical robustness of the SRI estimates with respect to digitization uncertainty, each dataset was subjected to a Monte Carlo perturbation procedure implemented in R. For each realization, random Gaussian noise with zero mean was added independently to the response variable values of both wetting and drying branches, after which the full calculation chain was repeated, including interpolation, resampling, area calculation, and normalization. The mean SRI and its standard deviation were then obtained from 1000 realizations for each case, using a fixed random seed to ensure reproducibility.

The perturbation amplitude σ was adapted to the scale and graphical resolution of each dataset.

Specifically, σ values were selected to represent approximately 1% of the total response-axis range in each dataset, consistent with the typical digitization uncertainty of WebPlotDigitizer for figures of the graphical resolution used in the source studies. This criterion yielded $\sigma = 0.5$ for datasets expressed in percentage units of volumetric water content

https://doi.org/10.3390/app16136667

(range ≈ 0–70%; sources [12,14]); σ = 0.005 for the Shein and Mady [13] dataset, where the response variable spans approximately 0.4 cm^3 cm^{-3}; and σ = 0.05 for the Arthur et al. [15,16] vapor sorption datasets, where this value represents a conservative upper bound on digitization error given the higher graphical resolution of the source figures. The robustness of SRI estimates to this choice is demonstrated a posteriori by the small standard deviations obtained (SD $\leq$ 5% of the corresponding mean in all cases), confirming that the results are not sensitive to the precise amplitude of the perturbation within the plausible range of digitization uncertainty.

The Monte Carlo analysis was not intended to represent experimental measurement uncertainty in a strict metrological sense, but rather to test the stability of the SRI calculation with respect to plausible perturbations introduced by graphical data extraction. The reported standard deviations therefore quantify the numerical sensitivity of the index to the digitization-and-processing workflow.

3.6. Reproducibility and Implementation

All calculations were performed in R using custom scripts written for each literature dataset, while preserving a common computational structure across cases. In every script, the same workflow was applied: import of digitized data, identification of wetting and drying branches, optional log10 transformation of the forcing axis, interpolation onto a common grid, trapezoidal integration of branch divergence, normalization of the hysteresis area, and Monte Carlo propagation of digitization noise. All scripts are available from the corresponding author upon request.

4. Results and Discussion

4.1. Overview of SRI Values Across Datasets

The SRI values obtained from the analyzed datasets are reported in Table 1 and illustrated in Figure 2. The index spans more than one order of magnitude, ranging from 0.023 to 0.333, reflecting substantial variability in the degree of hydraulic path asymmetry across contrasting systems and experimental conditions.

4.2. Evolution of SRI Under Repeated Wetting–Drying Cycling

The dataset reported by Wen et al. [14] for a Guangxi Guiping Clay (GGC) subjected to five consecutive wetting–drying cycles provides a particularly clear illustration of the sensitivity of SRI to structural history. The index decreases monotonically from 0.333 in the first cycle to 0.023 in the fifth, a reduction of approximately one order of magnitude over the course of the experiment (Table 1 and Figure 2).

This progressive decline reflects a systematic attenuation of path asymmetry as the system is subjected to repeated hydraulic forcing. From a structural standpoint, the result is consistent with the well-documented conditioning effect of cyclic wetting and drying, which promotes progressive reorganization of the pore network, the elimination of metastable configurations, and a convergence of the drying and wetting trajectories toward a more reversible hydraulic response [3,6].

Within the SRI framework, this trajectory corresponds to a transition from a state characterized by strong path dependence and pronounced structural memory toward a dynamically stabilized regime in which the system responds more symmetrically to forward and backward hydraulic forcing. The near-zero value attained after the fifth cycle (SRI = 0.023 $\pm$ 0.005) indicates that path asymmetry has been largely suppressed and the hysteresis loop substantially closed. Notably, the rate of SRI decline is not uniform: the largest reduction occurs between the first and third cycles (from 0.333 to 0.130), while the fourth and fifth cycles show progressively smaller decrements, suggesting an asymptotic approach toward a residual level of irreversibility that persists even after extensive hydraulic conditioning.

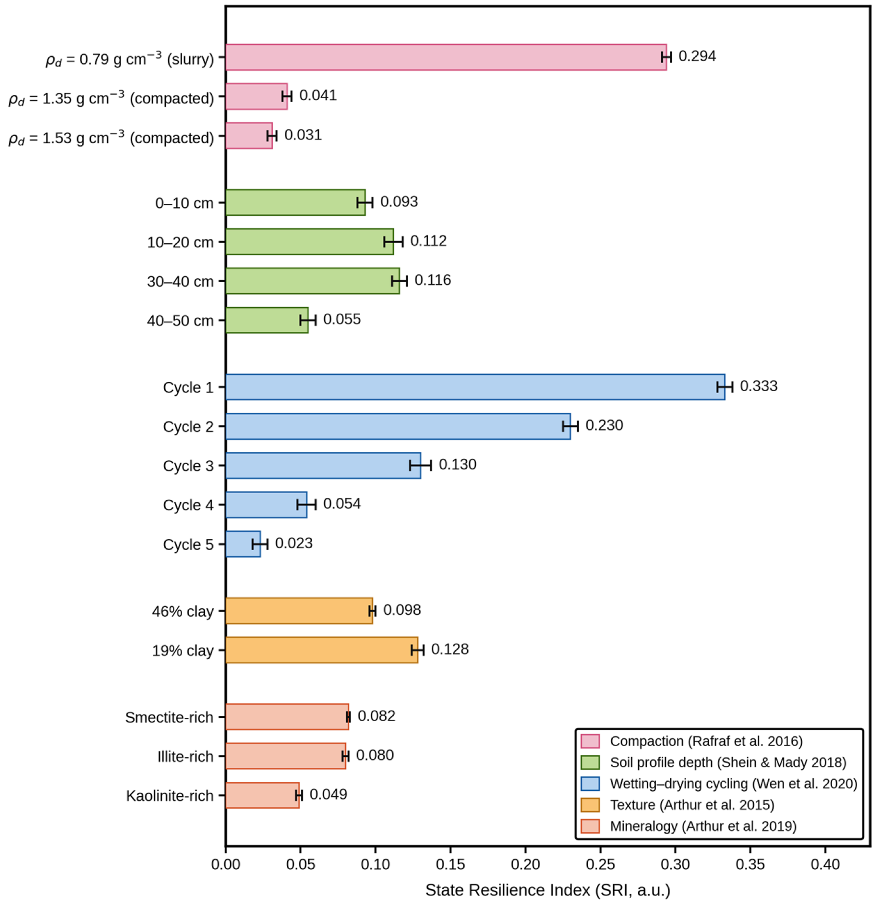

Figure 2. State Resilience Index (SRI) values obtained from digitized hysteresis datasets across five contrasting pedophysical drivers. Error bars represent standard deviations from Monte Carlo simulations (N = 1000). Color coding identifies the reference study: pink, Rafraf et al. [12]; green, Shein and Mady [13]; blue, Wen et al. [14]; amber, Arthur et al. [15]; orange, Arthur et al. [16].

This behavior carries direct implications for soil health interpretation. The progressive convergence of drying and wetting trajectories implies a reduction in the capacity of the pore network to retain water along distinct pathways under changing boundary conditions. As SRI approaches zero, the soil loses structural complexity in the hydraulic sense: its water retention behavior becomes increasingly symmetric and less sensitive to the direction of the hydraulic forcing. This homogenization of pore response may be interpreted as a deterioration of the soil's capacity to sustain differential water availability across the moisture cycle, with potential consequences for plant-available water storage and microbial habitat diversity.

4.3. Effect of Compaction on Hydraulic Path Asymmetry

The dataset reported by Rafraf et al. [12] for a silt loam soil at three bulk densities—slurry (ρ_d = 0.79 g cm^{-3}), moderately compacted (ρ_d = 1.35 g cm^{-3}), and heavily compacted (ρ_d = 1.53 g cm^{-3})—reveals a sharp reduction in SRI with increasing bulk density. The index decreases from 0.294 in the slurry state to 0.041 and 0.031 in the two compacted conditions, respectively (Table 1 and Figure 2).

This near-tenfold reduction reflects the progressive restriction of pore space and the associated loss of structural flexibility under mechanical loading. In the slurry state, the pore network is dominated by a wide distribution of pore sizes and geometries, with substantial capacity for metastable configurations to arise during drying and to be resolved differently during rewetting. As bulk density increases, macropores are progressively eliminated, the pore size distribution becomes more uniform, and the divergence between drying and wetting trajectories is correspondingly suppressed.

From the perspective of SRI, compaction acts as a structural constraint that reduces the accessible phase space available for path-dependent responses. The index captures this effect in a normalized and variable-independent manner, providing a compact quantification of what compaction does to the soil's structural memory. It is important to emphasize, however, that low SRI values in this context are not indicative of improved hydraulic functioning. Rather, they reflect a diminished capacity for structural adjustment under changing moisture conditions—a consequence that, under field conditions, may manifest as reduced buffering of water availability and increased vulnerability to rapid drying.

4.4. Depth-Dependent Structural Complexity and the Non-Monotonic SRI Profile

The data reported by Shein and Mady [13] for four distinct horizons of a Russian agricultural soil reveal a non-monotonic depth pattern in SRI, with values of 0.093, 0.112, 0.116, and 0.055 for the 0–10, 10–20, 30–40, and 40–50 cm layers, respectively (Table 1 and Figure 2). Bulk density increases monotonically with depth, from 1.18 to 1.49 g cm^{-3}. The soil studied by Shein and Mady [13] was an agricultural sod-podzolic silty clay loam sampled from three genetically distinct horizons: the cultivated Ap horizon (0–30 cm, subdivided into layers at 0–10, 10–20, and 20–30 cm, the latter affected by historical deep tillage in the 1960s), the eluvial EL horizon (30–40 cm, with BEL fragments and BELh morphons), and the illuvial BT1 horizon (40–50 cm), which forms a continuous clay-enriched layer. The overall mean clay and silt contents were 25.5% and 70.3%, respectively, with considerable variability across the profile. This pedogenic differentiation implies that each sampled layer represents a distinct structural environment, not merely a compaction state of the same parent material.

At first glance, this pattern might appear inconsistent with the trend observed in Rafraf et al. [12], where increasing bulk density was associated with decreasing SRI. However, the two datasets differ in a fundamental respect: whereas in Rafraf et al. [12] the same material was subjected to mechanical compaction under controlled laboratory conditions—with bulk density as the sole variable—in Shein and Mady [13] the compared units are distinct soil horizons, each characterized by a different combination of texture, clay content, organic matter, and aggregate structure. In this context, bulk density is not an independent variable, but a covarying property that co-evolves with the full suite of pedogenic characteristics of each horizon. It is also worth noting that the hysteresis indices reported by Shein and Mady [13] are derived from fitted parametric models and evaluated at specific points of the retention curve, whereas SRI integrates the full divergence between branches over their common domain. The two descriptors are therefore not expected to rank systems identically, and discrepancies of this kind are informative rather than contradictory: they reflect the different aspects of hysteretic behavior that each metric captures.

The SRI values therefore reflect the integrated structural complexity of each horizon rather than the effect of density alone. The horizons at 10–20 cm (SRI = 0.112) and 30–40 cm (SRI = 0.116), which show the highest values in the profile, correspond to the Ap lower sublayer and the eluvial EL horizon—zones that, in sod-podzolic soils, are typically characterized by relatively higher clay and organic matter contents compared to the surface cultivated layer, and by pedogenic processes (eluviation, clay translocation) that generate structurally heterogeneous pore networks with greater capacity for path-dependent hydraulic responses [13]. This is consistent with the general pedogenic description reported [13] and with the known behavior of sod-podzolic soils in the literature [17,18].

The surface horizon (0–10 cm; SRI = 0.093) may be influenced by tillage disturbance and seasonal wetting—drying cycles that partially homogenize its structure. The deepest horizon (40–50 cm; SRI = 0.055), corresponding to the illuvial BT1 layer, likely exhibits lower SRI because its structural organization is dominated by more uniform packing and reduced biopore activity. In this context, biopores refer to cylindrical macropores formed by decaying roots and soil fauna galleries, which—where present in shallower horizons—generate geometrically irregular pore networks that amplify divergence between wetting and drying paths; at the depths characteristic of the BT1 horizon, biological colonization is substantially reduced, limiting this source of pore-scale heterogeneity.

This interpretation is consistent with the conceptual framework of SRI as a descriptor of structural heterogeneity in the hydraulic sense: systems in which the pore network supports a broader range of configurations will exhibit greater path asymmetry and therefore higher SRI, regardless of the specific physical mechanism responsible for that heterogeneity.

4.5. Textural and Mineralogical Controls on Vapour Sorption Hysteresis

The water vapor sorption datasets provide an opportunity to extend the application of SRI beyond the capillary-dominated regime of the soil water retention curve, into the hygroscopic range where adsorption and desorption isotherms diverge at low relative humidity. Two complementary studies are considered here.

The dataset of Arthur et al. [15] includes two soils with contrasting clay contents—46% and 19%—both measured under identical experimental conditions. The SRI values obtained are 0.098 ± 0.002 and 0.128 ± 0.004, respectively (Table 1 and Figure 2). The higher SRI for the coarser-textured soil is counterintuitive if interpreted solely in terms of clay content, as finer soils are generally expected to exhibit greater water sorption hysteresis in absolute terms. However, the normalization inherent in the SRI formulation re-frames this comparison: what the index quantifies is not the absolute area of the hysteresis loop, but its magnitude relative to the accessible phase space defined by the dynamic range of both the forcing variable and the observable response. In the 46% clay soil, the large absolute water contents dominate both the loop area and the response range, resulting in partial compensation and a lower normalized index. In contrast, the 19% clay soil—characterized by a more heterogeneous pore size distribution arising from the coexistence of sand, silt, and clay fractions—exhibits a hysteresis loop that occupies a proportionally larger fraction of the accessible phase space. This interpretation is consistent with the broader principle that normalization can invert rankings relative to absolute loop areas when the dynamic ranges of the systems differ substantially.

The dataset of Arthur et al. [16] enables a direct comparison of three soil samples with identical clay content (45%) but contrasting mineralogy: smectite-rich, illite-rich, and kaolinite-rich. The SRI values are 0.082 ± 0.001, 0.080 ± 0.002, and 0.049 ± 0.002, respectively (Table 1 and Figure 2). The kaolinite-rich sample shows a distinctly lower SRI, consistent with the behavior reported for this mineral in the water vapor sorption literature: kaolinite exhibits a Type III isotherm shape, with minimal hysteresis across most of the relative humidity range and a sharp water uptake only at high relative humidity associated with capillary condensation in inter-particle pores [16]. The rigid, non-expandable structure of kaolinite limits the capacity for interlayer rearrangement during adsorption and desorption, thereby suppressing path asymmetry and yielding a correspondingly low SRI. The smectite-rich and illite-rich samples, by contrast, show similar and higher SRI values, reflecting their greater structural flexibility and the involvement of interlayer hydration processes that introduce distinct forward and backward pathways in the sorption cycle.

That smectite and illite yield nearly indistinguishable SRI values (0.082 and 0.080) deserves comment. From a mineralogical standpoint, smectite would generally be expected to exhibit more pronounced hysteresis than illite due to its greater expandability and interlayer cation hydration activity. However, SRI is a normalized descriptor, and normalization by the full dynamic range of the response may partially offset the larger absolute hysteresis of smectite relative to illite when the two systems differ appreciably in their total water sorption capacity. The near-equivalence of the two values therefore does not imply that smectite and illite behave identically at the pore scale; rather, it reflects the fact that, once expressed as a fraction of the accessible phase space, their path asymmetries are comparable under the specific experimental conditions represented in this dataset. Resolving this distinction would require datasets with finer graphical resolution or access to raw measurement data.

From a soil quality perspective, these mineralogical contrasts carry a direct interpretive implication. The low SRI of the kaolinite-rich sample does not reflect poor water retention in absolute terms but indicates that the adsorption and desorption paths are nearly symmetric—the system has limited structural memory. Soils dominated by kaolinite, common in strongly weathered tropical and subtropical environments, therefore exhibit reduced capacity to buffer water availability across wetting and drying episodes relative to soils with similar clay contents but smectitic or illitic mineralogy. The SRI framework thus reveals a mineralogically driven dimension of soil functional resilience that is not captured by clay content alone, and which may be relevant for the interpretation of water availability under variable rainfall regimes.

4.6. Unified Interpretation and Reference Framework for SRI

Taken together, the results across all five datasets demonstrate that SRI responds consistently and mechanistically to the dominant drivers of hydraulic path asymmetry. High values (>0.2) are observed in systems characterized by pronounced structural reconfiguration or metastable initial configurations—such as slurry conditions and early wetting–drying cycles. Intermediate values (≈0.05–0.15) are associated with structured soils under natural pedogenic conditions, where hysteresis arises from moderate pore heterogeneity and interactions with organic matter and clay. Low values (<0.05) characterize systems in which structural constraints—whether imposed mechanically through compaction, through mineralogical rigidity, or through progressive pore network stabilization under repeated hydraulic cycling—limit the divergence between forward and backward trajectories.

These ranges should be regarded as indicative and context-dependent rather than fixed thresholds. Similar SRI values may in principle arise from different physical mechanisms, and the index cannot, by itself, decompose the contributions of individual sources of hysteresis. Its interpretive value therefore increases when used in conjunction with complementary information on soil structure, texture, mineralogy, and land management history, rather than as a standalone predictor.

It should also be noted that SRI requires both drying and wetting branches of the hysteresis loop to be available. In contexts where only the drying branch has been measured—as is common in large-scale soil hydraulic databases—SRI cannot be computed directly. In such cases, existing parametric approaches for wetting branch reconstruction from drying curve parameters—such as the scaling procedure proposed by Kool and Parker [19]—may be applied as a pre-processing step, although the associated uncertainty should be propagated into the SRI estimate.

SRI functions as a diagnostic and comparative descriptor: it quantifies the degree of path asymmetry encoded in a measured hysteresis loop, but does not forecast water content trajectories under arbitrary boundary conditions. Predictive simulation of soil water dynamics remains the domain of parametric constitutive models such as those of Kool and Parker [19], which SRI complements by supplying a normalized, model-free summary of the structural information contained in the loop.

Importantly, the framework introduced here is not restricted to the capillary-dominated range of the soil water retention curve. The consistent behavior of SRI across both matric potential and water vapor sorption datasets—covering forcing ranges that span from near-saturation to hygroscopic conditions—demonstrates that the index is transferable across observational scales and measurement domains. This property, combined with its computational transparency and freedom from parametric assumptions, positions SRI as a broadly applicable tool for the comparative characterization of path-dependent hydraulic behavior in soils and related porous materials.

5. Conclusions

This study has demonstrated that the State Resilience Index (SRI) constitutes a robust, dimensionless, and transferable descriptor of hydraulic path asymmetry in soils, applicable across a wide range of systems, forcing regimes, and measurement scales. By normalizing the area enclosed between drying and wetting trajectories against the accessible phase space of the system, SRI provides a compact and physically interpretable summary of the degree to which a soil retains the imprint of its prior hydraulic states. Across the five datasets analyzed—encompassing compaction gradients, repeated wetting–drying cycles, depth-resolved soil profiles, and water vapor sorption isotherms from soils differing in texture and clay mineralogy—the index responded consistently and mechanistically to the dominant structural drivers of hysteresis, spanning more than one order of magnitude from near-reversible to strongly path-dependent conditions.

Beyond its descriptive utility, SRI carries interpretive value as an indicator of soil structural quality. As the case-by-case analysis has shown, systems with higher SRI values sustain more heterogeneous pore architectures, greater buffering of plant-available water, and broader microhabitat diversity for soil biota. Conversely, declining SRI—whether driven by compaction, repeated hydraulic cycling, or mineralogical homogeneity—signals a progressive convergence of drying and wetting paths that is functionally consistent with structural degradation. The monitoring of SRI across management treatments or over time could therefore serve as an early-warning indicator of soil health trajectories, complementing existing physical and biological indices. It should be emphasized that SRI does not quantify geometric features of the hysteresis loop per se, but rather the fraction of thermodynamic work irreversibly dissipated per cycle relative to the maximum accessible under the given experimental conditions, as formally derived in Section 2. The interpretive connection to soil structural quality therefore rests on thermodynamic reasoning rather than on curve geometry alone. Nevertheless, direct validation of this connection against independent structural measurements—such as pore-size distribution, X-ray CT imaging, or aggregate stability indices—remains a necessary step before SRI can be used as a quantitative soil health indicator in applied monitoring contexts and represents an important direction for future research.

The provisional interpretive framework proposed in the preceding section—with SRI values above 0.2 indicative of high structural resilience, values in the range 0.05–0.15 characteristic of structured agricultural soils under moderate management pressure, and values below 0.05 associated with structurally constrained conditions—provides an empirical reference for comparative assessment. Its calibration against independent measures of soil health and crop productivity across specific pedoclimatic contexts remains an important direction for future research.

https://doi.org/10.3390/app16136667

Several limitations of the present study should be acknowledged. The SRI values reported here are derived from digitized published figures rather than raw experimental data, introducing a source of uncertainty that has been quantified through Monte Carlo analysis but cannot be entirely eliminated. Furthermore, the datasets analyzed represent a limited and purposefully selected set of contrasting cases, and the generalizability of the proposed interpretive framework to a broader range of soil types, climatic regimes, and land use histories requires systematic empirical validation. Future work should also explore the sensitivity of SRI to measurement protocol—including the range and resolution of the forcing variable, the number of equilibration points, and the direction of the first hydraulic path—as well as its relationship to independently measured indicators of soil structural quality such as aggregate stability, air permeability, and biological activity indices. It should also be noted that SRI requires both the drying and wetting branches of the hysteresis loop to be available. In contexts where only the drying branch has been measured—as is common in large-scale soil hydraulic databases—SRI cannot be computed directly. In such cases, existing parametric approaches for wetting branch reconstruction from drying curve parameters [19] may be applied as a pre-processing step, although the associated uncertainty should be propagated into the SRI estimate.

In conclusion, the State Resilience Index provides a physically grounded, computationally transparent, and transferable tool for the characterization of soil hydraulic behavior. Its sensitivity to structural state, its responsiveness to degradation processes, and its applicability across measurement domains position it as a promising addition to the toolkit of soil quality assessment, complementing existing physical and biological indicators with a uniquely integrative descriptor of the soil's structural memory and path-dependent response. SRI is designed as a diagnostic and comparative descriptor, not as a predictive tool for soil water flux modelling. Its value lies in characterizing the degree of path asymmetry embedded in measured hysteresis loops, rather than in forecasting water content trajectories under arbitrary boundary conditions. Applications requiring predictive simulation of soil water dynamics should continue to rely on parametric constitutive models [19]. SRI complements these frameworks by providing a normalized, thermodynamically grounded summary of the structural information encoded in the hysteresis loop.

Funding: This research received no external funding.

Institutional Review Board Statement: Not applicable.

Informed Consent Statement: Not applicable.

Data Availability Statement: The digitized datasets and R scripts analyzed during this study are available from the corresponding author upon reasonable request.

Acknowledgments: During the preparation of this manuscript, the author used Generative AI (Claude.ai Sonnet 4.6) to write the R codes necessary for the data elaboration. The author has reviewed and edited the output and takes full responsibility for the content of this publication.

Conflicts of Interest: The author declares no conflicts of interest.

References

1. Mualem, Y. A Conceptual Model for Hysteresis. *Water Resour. Res.* **1974**, *10*, 514–520. [CrossRef]
2. Hillel, D. *Environmental Soil Physics*, 1st ed.; Academic Press—Elsevier: London, UK, 1998; ISBN 978-0-12-348525-0.
3. Pham, H.Q.; Fredlund, D.G.; Barbour, S.L. A Study of Hysteresis Models for Soil-Water Characteristic Curves. *Can. Geotech. J.* **2005**, *42*, 1548–1568. [CrossRef]
4. van Genuchten, M.T. A Closed-Form Equation for Predicting the Hydraulic Conductivity of Unsaturated Soils. *Soil Sci. Soc. Am. J.* **1980**, *44*, 892–898. [CrossRef]

https://doi.org/10.3390/app16136667

5. Gebrenegus, T.; Ghezzehei, T.A. An Index for Degree of Hysteresis in Water Retention. *Soil Sci. Soc. Am. J.* **2011**, *75*, 2122–2127. [CrossRef]
6. Tuller, M.; Or, D. Water Films and Scaling of Soil Characteristic Curves at Low Water Contents. *Water Resour. Res.* **2005**, *41*, W09403. [CrossRef]
7. Gao, Y.; Li, Z.; Sun, D.; Yu, H. A Simple Method for Predicting the Hydraulic Properties of Unsaturated Soils with Different Void Ratios. *Soil Tillage Res.* **2021**, *209*, 104913. [CrossRef]
8. Kramer, I.; Bayer, Y.; Adeyemo, T.; Mau, Y. Hysteresis in Soil Hydraulic Conductivity as Driven by Salinity and Sodicity-a Modeling Framework. *Hydrol. Earth Syst. Sci.* **2021**, *25*, 1993–2008. [CrossRef]
9. Likos, W.J.; Lu, N.; Godt, J.W. Hysteresis and Uncertainty in Soil Water-Retention Curve Parameters. *J. Geotech. Geoenviron. Eng.* **2014**, *140*, 04013050. [CrossRef]
10. Berthier, L.; Biroli, G. Theoretical Perspective on the Glass Transition and Amorphous Materials. *Rev. Mod. Phys.* **2011**, *83*, 587–645. [CrossRef]
11. Prigogine, I. *Introduction to Thermodynamics of Irreversible Processes*, 3rd ed.; Wiley: New York, NY, USA, 1967.
12. Rafraf, S.; Guellouz, L.; Guiras, H.; Bouhlila, R. Quantification of Hysteresis Effects on a Soil Subjected to Drying and Wetting Cycles. *Int. Agrophys.* **2016**, *30*, 493–499. [CrossRef]
13. Shein, E.V.; Mady, A.Y. Hysteresis of the Water Retention Curve: Wetting Branch Simulation Based on the Drying Curve. *Mosc. Univ. Soil Sci. Bull.* **2018**, *73*, 124–128. [CrossRef]
14. Wen, T.; Shao, L.; Guo, X.; Zhao, Y. Experimental Investigations of the Soil Water Retention Curve under Multiple Drying–Wetting Cycles. *Acta Geotech.* **2020**, *15*, 3321–3326. [CrossRef]
15. Arthur, E.; Tuller, M.; Moldrup, P.; Jensen, D.K.; De Jonge, L.W. Prediction of Clay Content from Water Vapour Sorption Isotherms Considering Hysteresis and Soil Organic Matter Content. *Eur. J. Soil Sci.* **2015**, *66*, 206–217. [CrossRef]
16. Arthur, E.; Tuller, M.; Norgaard, T.; Moldrup, P.; de Jonge, L.W. Improved Estimation of Clay Content from Water Content for Soils Rich in Smectite and Kaolinite. *Geoderma* **2019**, *350*, 40–45. [CrossRef]
17. Shishov, L.L.; Tonkonogov, V.D.; Gerasimova, M.I.; Lebedeva, I.I. New Classification System of Russian Soils. *Eurasian Soil Sci.* **2005**, *38*, S35–S43.
18. Zaidel'man, F.R.; Shvarov, A.P.; Ginzburg, T.M. Genesis, Hydrology, and Properties of Soils in Mesodepressions Waterlogged by Surface Water in the Northern Ryazan Forest-Steppe. *Eurasian Soil Sci.* **2007**, *40*, 917–927. [CrossRef]
19. Kool, J.B.; Parker, J.C. Development and Evaluation of Closed-form Expressions for Hysteretic Soil Hydraulic Properties. *Water Resour. Res.* **1987**, *23*, 105–114. [CrossRef]